Inorganica Chimica Acta 492 (2019) 76–82

Contents lists available at ScienceDirect

Inorganica Chimica Acta

journal homepage: www.elsevier.com/locate/ica

Research paper

Synthesis, structures and catalase activities of bis(μ-oxo)diMn^{III,III} and bis(μ-acetato)diMn^{II,II} complexes bearing a quinolyl donor tripod ligand

Sachidulal Biswas[a], Purak Das[b], Sagarmani Rasaily[c], Anand Pariyar[c], Achintesh Narayan Biswas[a,*]

[a] Department of Chemistry, National Institute of Technology Sikkim, Ravangla, South Sikkim 737139, India
[b] Department of Chemistry, Rishi Bankim Chandra College for Women, Naihati 743165, India
[c] Department of Chemistry, Sikkim University, Sikkim 737102, India

ARTICLE INFO

Keywords:
Catalase mimics
Manganese
Tripodal ligand
Kinetics

ABSTRACT

The syntheses and characterization of two new complexes, $[Mn_2(TQA)_2(\mu\text{-}O)_2](ClO_4)_2$ (**1**) and $[Mn_2(TQA)_2(\mu\text{-}OAc)_2](ClO_4)_2$ (**2**) (TQA = tris(2-quinolylmethyl)amine), are described. The diMn complexes (**1** & **2**) have been characterized by elemental analysis, IR and X-ray diffraction. The complexes partly resemble the active-site structures of the oxidized and reduced forms of bacterial manganese catalases. Addition of aqueous H_2O_2 to the complexes in 1:1 MeOH/tris-buffer solution led to rapid evolution of O_2 confirming their catalase activity. The complexes **1** & **2** exhibited turnovers of 810 and 665 mol O_2 per mol of the catalysts, respectively. Catalytic efficiencies (k_{cat}/K_M) of 8.5 and 22 $M^{-1}s^{-1}$ were measured for the complexes **1** & **2**. The corresponding mononuclear Mn(II) complex, $[Mn(TQA)(MeCN)(ClO_4)](ClO_4)\cdot MeCN$ (**3**) also exhibited similar catalase activity. The complexes (**1**–**3**) showed marked preference for catalytic H_2O_2 disproportionation over oxidation of 2,2′-azinobis-(3-ethylbenzothiazoline)-6-sulfonicacid (ABTS).

1. Introduction

Despite being an essential bio-relevant metal ion, relatively few manganese based enzymes having a well characterized active site have been isolated till date. The most important physiological role played by the manganese is its involvement in the oxygen evolving complex (OEC) during photosynthesis [1–3]. Apart from this, a number of mononuclear (*viz.*, superoxide dismutase and manganese dioxygenase) and binuclear (*e.g.* Catalase, ribonucleotide reductase, arginase) manganese-containing enzymes have been isolated and characterized structurally during the last few decades [4–14]. Among them, manganese catalases are the most extensively studied [8–12]. Broadly, three different varieties of catalases that protect cells from harmful effects of H_2O_2 by converting it into water and dioxygen, have been identified. Among them, the iron-containing enzymes (heme-type catalase & chloroperoxidase) are most extensively studied [15]. The third variety of catalases isolated and characterized by protein crystallography from three bacterial organisms, *Lactobacillus plantarum* [16], *Thermus thermophiles* [17] and *Thermoleophilum* album [10] are found to contain dimanganese active sites. The enzymes cycle between Mn^{II}/Mn^{II} and Mn^{III}/Mn^{III} redox states during catalytic turnovers. Moreover, the oxidized and reduced forms of the enzymes differ in the nature of the bridging ligands. The oxidized form of the enzyme reveals an active site containing two Mn^{III} ions bridged by the carboxylate group of a glutamate residue in a *syn-syn* fashion. The motif is completed by two more bridging oxygen atoms, one of which is thought to be a μ-oxido [16]. In contrast, the reduced form of the enzyme features a μ-OH and a μ-OH_2 along with the bridging carboxylate unit [16].

Considerable efforts have been made to develop synthetic mimics of Mn-catalases as pharmaceutical agents to destroy H_2O_2 and other reactive oxygen species (ROS) [18–20]. So far, only a handful of functional mimics featuring diMn motifs have been reported [21–28]. A series of diMn complexes bearing binucleating salen type of ligands has emerged as efficient functional mimics. One of these, $[Mn^{IV}salpn(\mu\text{-}O)]_2$ (salpn = 1,3-bis(salicylideneamino)propane) exhibited excellent activity towards H_2O_2 disproportionation ($k_{cat} = 2.5 \times 10^2\ s^{-1}$) [29,30]. However, unlike the native enzymes, the catalyst cycles between $Mn^{IV}Mn^{IV}$ and $Mn^{III}Mn^{III}$ redox states. Another design strategy employed to synthesize diMn catalase mimics is to employ tripodal ligands offering two vacant *cis*-coordination sites upon metalation. These vacant coordination sites facilitate the synthesis of binuclear complexes. Triller et al. exploited this strategy and utilized a tripodal ligand bpia (bpia = bis(picolyl)(*N*-methylimidazol-2-yl)amine) to synthesize diMn catalase mimics [31]. The diMn(II/II) complex $[Mn_2(bpia)_2(\mu\text{-}OAc)_2]^{2+}$

* Corresponding author.
E-mail address: achintesh@nitsikkim.ac.in (A.N. Biswas).

https://doi.org/10.1016/j.ica.2019.04.015
Received 21 January 2019; Received in revised form 2 April 2019; Accepted 2 April 2019
Available online 10 April 2019
0020-1693/

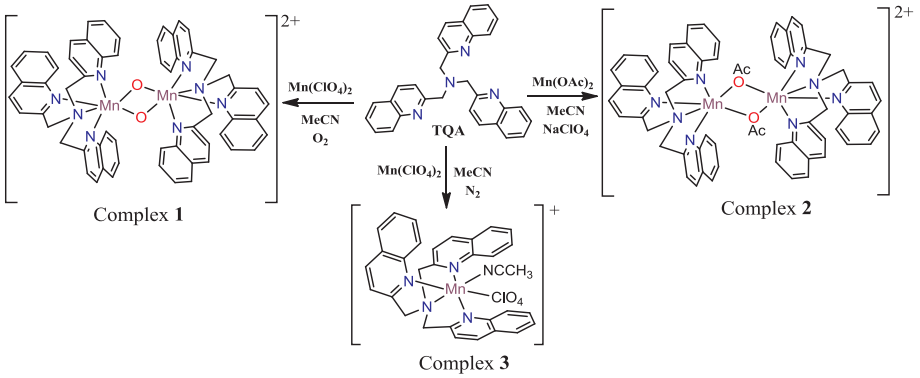

Scheme 1. Synthetic scheme of the metal complexes (**1–3**) used in this study.

mimicking the active site of the reduced form of manganese catalases has shown catalase activity (k_{cat} = 0.237 s^{-1}) [31,32].

In the present work, we have employed a tripodal ligand TQA (TQA = tris(2-quinolylmethyl)amine) to develop manganese catalase models. Despite being a member of the TPA family of ligands (TPA = tris(2-pyridylmethyl)amine), metal complexes bearing TQA have exhibited unique magnetic properties and unprecedented reactivity towards C–H bonds, attributable primarily to the greater steric bulk of quinolenes. In particular, the oxoiron(IV) complex of TQA has emerged as the best electronic functional model of the oxoiron(IV) intermediate of the enzyme TauD-*J* [33]. The complex featuring an S = 2 ground state exhibited unprecedented reactivity towards strong C–H bonds with rates of substrate oxidation 3–4 orders of magnitude larger than the related low-spin (S = 1/2) oxoiron(IV) complexes. The amazing reactivity pattern of the Fe-TQA complexes prompted us to explore the corresponding manganese complexes. Herein, we report the synthesis, characterization and reactivity of the complexes $[Mn_2(TQA)_2(\mu\text{-}O)_2](ClO_4)_2$ (**1**), $[Mn_2(TQA)_2(\mu\text{-}OAc)_2](ClO_4)_2$ (**2**) and $[Mn(TQA)(MeCN)(ClO_4)](ClO_4)\cdot MeCN$ (**3**) (Scheme 1). Complexes **1** and **2** are the approximate structural mimics of the oxidized and reduced form of the native manganese catalases. All the complexes have been shown to exhibit catalase activity at ambient conditions with excellent turnovers.

2. Experimental section

2.1. Materials and methods

All reagents were used as purchased from commercial suppliers. Solvents were purified by standard methods. The concentration of H_2O_2 stock solution was determined by iodometric titration. The ligand was prepared by previously reported method [34].

2.2. Synthesis of the manganese complexes

2.2.1. Synthesis of $[Mn_2(TQA)_2(O)_2](ClO_4)_2$ (1)

A mixture of $Mn(ClO_4)_2\cdot 6H_2O$ (180 mg, 0.5 mmol) and TQA (220 mg, 0.5 mmol) in 5 mL acetonitrile was stirred for 2 days in presence of air at room temperature. The yellow solution formed after 2 days of stirring was left under air for 7 days and brown crystalline solid separated out. The brown solid thus obtained was washed with ether and dried to get the desired complex. Suitable crystal for X-ray crystallography (dimension = 0.32 × 0.30 × 0.29 mm) were obtained by diffusion of diethyl ether to an acetonitrile solution of the catalyst. Yield: 250 mg (40%); Anal. Calc. for $C_{60}H_{48}Cl_2Mn_2N_8O_{10}$: C, 58.98; H, 3.96; N, 9.17. Found: C, 58.88; H, 3.92; N, 9.12. ESIMS (positive ion mode, acetonitrile) *m/z*: 511.12 $[Mn_2(TQA)_2(\mu\text{-}O)_2]^{2+}$. FT-IR (KBR, ν cm^{-1}): 2360, 1612, 1514, 1120.

2.2.2. Synthesis of $[Mn_2(TQA)_2(OAc)_2](ClO_4)_2$ (2)

A mixture of $Mn(OAc)_2\cdot 4H_2O$ (122 mg, 0.5 mmol) and TQA (220 mg, 0.5 mmol) was stirred for two hours in a vial containing 2 mL acetonitrile. Sodium perchlorate (1.0 mmol) was added to the reaction mixture. The solution was filtered and crystallized via vapour diffusion of diethyl ether to afford white crystals suitable for X-ray crystallography. Yield: 330 mg (50%). Anal. Calc. for $C_{64}H_{58}Cl_2Mn_2N_8O_{14}$: C, 57.19; H, 4.35; N, 8.34. Found: C, 57.14; H, 4.28; N, 8.28 ESIMS (positive ion mode, acetonitrile) *m/z*: 554.1 $[Mn_2^{II}(TQA)_2(OAc)_2]^{2+}$. FT-IR (KBr, ν cm^{-1}): 2360, 1598, 1511, 1116.

2.2.3. Synthesis of $[Mn(TQA)(CH_3CN)(ClO_4)](ClO_4)$ (3)

An acetonitrile solution of $Mn(ClO_4)_2\cdot 6H_2O$ (180 mg, 0.5 mmol) was added dropwise to a vial containing TQA (220 mg, 0.5 mmol) in 2 mL acetonitrile under N_2. The reaction mixture was stirred for 30 min at room temperature. The solution was then poured onto diethyl ether to get a white precipitate. Suitable crystal for X-ray crystallography (dimension = 0.28x 0.26 × 0.23 mm) were obtained by diffusion of diethyl ether to an acetonitrile solution of the catalyst. Yield: 290 mg (81%). Anal. Calc. for $C_{34}H_{30}C_{l2}MnN_6O_8$: C, 52.59; H, 3.89; N, 10.82. Found: C, 52.54; H, 3.85, N, 10.76. ESIMS (positive ion mode, acetonitrile) *m/z*: 594.32 $[Mn^{II}(TQA)(ClO_4)]^+$. FT-IR (KBr, ν cm^{-1}): 1601, 1514, 1433, 1126, 830.

2.3. Physical and analytical measurements

FT-IR spectra were recorded on a JASCO FT/IR-4700 spectrophotometer. Mass spectra were recorded on a Bruker micro-TOF MS-Agilent series 1200 LC using electron spray ionization mode.

2.4. X-ray crystallography

Crystallographic data and experimental details for all the three complexes are summarized in Tables 1 and 2. Data on the crystals were collected on a Bruker SMART 1000 CCD area-detector diffractometer using graphite monochromated Mo Kα (λ = 0.71073 Å) radiation by ω scan. The structure was solved by direct methods using SHELXS-97 and difference Fourier syntheses and refined with SHELXL-97 [35,36] package incorporated in WinGX 1.64 crystallographic collective package [37]. All the hydrogen positions for the compound were initially located in the difference Fourier map, and for the final refinement, the hydrogen atoms were placed geometrically and held in the riding mode. The last cycles of refinement included atomic positions for all the atoms, anisotropic thermal parameters for all non-hydrogen atoms and isotropic thermal parameters for all the hydrogen atoms. Full matrix-least-squares structure refinement against $|F^2|$. Molecular geometry calculations were performed withPLATON [38] and molecular graphics were prepared using ORTEP-3 [39]. SQUEEZE/PLATON was used in structural refinement in complex **2**. The unit cell contains 10

Table 1
Crystal data collection and structure refinement for complex **1**, **2** and **3**.

Crystal data	1	2	3
CCDC reference number	1888233	1888234	1888235
Empirical formula	$C_{60}H_{48}Cl_2Mn_2N_8O_{10}$	$C_{64}H_{58}Cl_2Mn_2N_8O_{14}$	$C_{34}H_{30}Cl_2MnN_6O_8$
Formula weight (g mol^{-1})	1221.85	1343.96	776.48
Crystal system	Monoclinic	Orthorhombic	Triclinic
Space group	*P* 21/*n*	*P* 21 21 21	*P* −1
Unit cell dimensions			
	a = 12.6077(6) Å	a = 14.3204(4) Å	a = 11.8279(4) Å
	α = 90°	α = 90°	α = 80.9452(2)°
	b = 17.9394(9) Å	b = 20.9301(6) Å	b = 16.2640(5) Å
	β = 101.59(3)°	β = 90°	β = 81.825(3)°
	c = 12.6858(6)	c = 22.3385(6)	c = 18.6633(6)
	γ = 90°	γ = 90°	γ = 74.534(3)°
Volume Å^3	2811.2(2)	6695.5(3)	3398.12(19)
Z	2	4	4
D (calculated), Mg/m^3	1.443	1.333	1.518
Absorption coefficient, mm^{-1}	0.612	0.525	5.135
Data collection			
Temperature, K	293(2)	293(2)	293(2)
Refinement			
[c]Goodness-of-fit on F^2 (GOF)	1.057	0.964	1.026
Final R indices [I > 2σ(I)]	R_1 = 0.0762,	R_1 = 0.0783	R_1 = 0.0447
	wR_2 = 0.1766	wR_2 = 0.1886	wR_2 = 0.1199
R indices (all data)	R_1 = 0.1146,	R_1 = 0.0931	R_1 = 0.0490,
	wR_2 = 0.1994	wR_2 = 0.2098	wR_2 = 0.1241

$R_1 = \Sigma F_{obsd} - F_{calcd}/\Sigma F_{obsd}$. $wR_2 = \{\Sigma[w(F_{obsd}{}^2 - F_{calcd}{}^2)^2]/\Sigma[w(F_{obsd}{}^2)^2]\}^{1/2}$.
GOF = $\{\Sigma[w(F_{obsd}{}^2 - F_{calcd}{}^2)^2]/n_{data} - n_{vari}\}^{1/2}$.

water molecules which have been treated as a diffuse contribution to the overall scattering without specific atom positions by SQUEEZE/PLATON. CCDC reference number 1888233 (complex **1**), 1888234 (complex **2**) and 1888235 (complex **3**) contains the supplementary crystallographic data for this paper. These data can be obtained free of charge from The Cambridge Crystallographic Data Centre (CCDC) *via* www.ccdc.cam.ac.uk/data_request/cif.

2.5. Study of catalase activity

Catalase activity of the complexes were measured at 293 K polarographically using a Clark-type electrode (Hansatech Oxygraph$^+$). Before each experiment the electrode was calibrated using air saturated water. Reactions were performed in 1:1 methanol:Tris-HCl buffer solution. After attaining a steady baseline, different amounts of H_2O_2 was added to the sealed reaction vessel containing the catalyst solution (0.1 mM). Initial rate method was used for kinetic studies and rates were determined by measuring the dissolved oxygen. In case of

Table 2
Selected bond lengths (Å), bond angles (°) and torsion angles (°) for complex **1**, **2** and **3**.

Bond lengths (Å)					
Complex **1**		Complex **2**		Complex **3**	
Mn(1)–O(1)′	1.824(3)	Mn(1)–O(11)	2.070(4)	Mn(1)–N(1)	2.231(2)
Mn(1)–O(1)	1.830(3)	Mn(1)–O(9)	2.129(4)	Mn(1)–N(2)	2.312(2)
Mn(1)–N(1)	2.114(4)	Mn(1)–N(1)	2.281(5)	Mn(1)–N(3)	2.242(2)
Mn(1)–N(3)	2.146(4)	Mn(2)–O(12)	2.148(4)	Mn(1)–N(4)	2.316(2)
Mn(1)–N(4)	2.361(4)	Mn(2)–O(10)	2.058(4)	Mn(1)–N(5)	2.160(2)
Mn(1)–N(2)	2.383(4)	Mn(1)–N(3)	2.323(5)	Mn(1)–O(1)	2.2746(18)
Mn(1)–Mn(1)′	2.6772(12)	Mn(2)–N(5)	2.264(5)	Cl(3)–O(11)	1.415(2)
O(1)–Mn(1)′	1.824(3)	Mn(2)–N(8)	2.280(5)	Cl(3)–O(12)	1.4378(18)
Bond angles (°)					
O(1)′–Mn(1)–O(1)	85.78(15)	O(11)–Mn(1)-O(9)	92.51(18)	N(5)–Mn(1)–N(1)	167.91(8)
O(1)′–Mn(1)–N(1)	175.62(15)	O(11)–Mn(1)–N(1)	169.3(2)	N(5)–Mn(1)–N(3)	111.74(8)
O(1)–Mn(1)–N(1)	89.87(15)	O(9)–Mn(1)–N(1)	87.44(17)	N(1)–Mn(1)–N(3)	80.06(7)
O(1)′–Mn(1)–N(3)	101.89(15)	O(11)–Mn(1)–N(3)	102.99(18)	N(5)–Mn(1)–O(1)	85.17(7)
O(1)–Mn(1)–N(3)	172.26(15)	O(9)–Mn(1)–N(3)	164.49(17)	N(1)–Mn(1)–O(1)	83.57(7)
O(1)′–Mn(1)–N(4)	105.19(16)	O(11)–Mn(1)–N(4)	115.75(19)	N(3)–Mn(1)–O(1)	161.24(7)
O(1)–Mn(1)–N(4)	94.56(15)	O(9)–Mn(1)–N(4)	95.35(18)	N(5)–Mn(1)–N(2)	102.00(8)
N(1)–Mn(1)–N(4)	74.57(17)	O(10)–Mn(2)–(12)	92.81(17)	N(1)–Mn(1)–N(2)	74.04(8)
N(3)–Mn(1)–N(4)	82.48(15)	O(12)–C(63)–O(11)	123.8(6)	N(3)–Mn(1)–N(2)	92.24(7)
O(1)′–Mn(1)–N(2)	106.69(16)	O(9)–C(61)–O(10)	122.9(5)	O(1)–Mn(1)–N(2)	92.00(7)
O(1)–Mn(1)–N(2)	94.51(15)	O(10)–Mn(2)–N(6)	97.81(19)	N(5)–Mn(1)–N(4)	106.80(8)
N(1)–Mn(1)–N(2)	74.18(18)	O(12)–Mn(2)–N(6)	85.59(18)	N(1)–Mn(1)–N(4)	75.91(8)
Mn(1)′–O(1)–Mn(1)	94.22(15)	N(8)–Mn(2)–N(6)	149.7(2)	N(3)–Mn(1)–N(4)	85.50(7)
O(1)′–Mn(1)–Mn(1)′	42.97(10)	N(7)–Mn(2)–N(6)	90.68(18)	O(1)–Mn(1)–N(4)	81.67(7)
O(1)–Mn(1)–Mn(1)′	42.81(10)	O(11)–Mn(1)–N(2)	97.8(2)	N(2)–Mn(1)–N(4)	149.81(8)

volumetric analysis, a 10 mL flask was used, sealed with a septum and connected to a burette having precision of 0.1 mL. The catalytic reaction was initiated by the introduction of H_2O_2 solution using a syringe to the catalyst solution (0.2 mM) and evolution of dioxygen was measured volumetrically.

2.6. Peroxidase probes

The following procedure was used for studying the oxidation of 2,2′-azinobis-(3-ethylbenzothiazoline)-6-sulfonicacid (ABTS) by the complexes with H_2O_2 at *ca.* pH 7. Methanolic solution of the catalyst (10 μL; 10^{-3} M; 10^{-8} mol) and an aqueous ABTS solution (50 μL; 0.009 M; 4.5×10^{-7} mol) were added to 3 mL water. To the above solution H_2O_2 (50 μL; 10 M; 5×10^{-4} mol) was added and the oxidation of ABTS started immediately. Oxidation of ABTS was followed by monitoring the increase in intensity of UV absorption bands.

3. Results and discussion

3.1. Synthesis of the complexes

The tripodal qunolyl ligand (TQA) was synthesized by literature method [34]. Reaction of equimolar amounts of TQA and Mn(II)-perchlorate in acetonitrile under air resulted in the formation of the bis(μ-oxo)bismanganese(III) complex, $[Mn_2(TQA)_2(\mu\text{-}O)_2](ClO_4)_2$ (**1**). Complex **1** has been thoroughly characterized by spectral analysis and X-ray crystallography (Fig. 1). The presence of Mn_2O_2 core motif is indicated by its FT-IR spectrum (Fig. S1), which exhibits a vibration at 670 cm^{-1}, a characteristic feature of the Mn_2O_2 core [40]. For the related complex $[Mn_2(TPA)_2(\mu\text{-}O)_2](ClO_4)_2$ (TPA = tris(2-pyridylmethyl)amine), Mn–μ-oxo vibration appears at 660 cm^{-1} [41]. ESI-MS data of the complex in acetonitrile exhibited a major peak at 511.12 *m/z*, which can be attributed to $[Mn_2(TQA)_2(\mu\text{-}O)_2]^{2+}$ (Fig. S2).

Finally, the coordination environments of the manganese centres were obtained from X-ray diffraction study. A thermal ellipsoid plot of the complex **1** together with the selective atom numbering scheme is illustrated in Fig. 1. Selected bond distances and angles are listed in Table S2. Complex **1** contains the Mn_2O_2 diamond core motif with the N4 ligand and thus provides a distorted octahedral environment around both manganese(III) centres. The planar Mn_2O_2 is characterized by an acute Mn–O–Mn angle (94.22°) and a short Mn–Mn distance (2.677 Å), which is slightly longer than that reported previously for the structurally related complex, $[Mn_2(O)_2(TPA)_2]^{2+}$. The Mn–μ-oxo bonds of **1** (Mn1–O1^1 = 1.824 Å and Mn1–O1 = 1.830 Å) are shorter than those of $[Mn_2(O)_2(TPA)_2]^{2+}$ [41]. The Mn–N bonds (Mn1–N1 = 2.114 Å and Mn1–N3 = 2.146 Å) *trans* to the bridging oxo is shortened by 0.2 Å from the other axial Mn–N bonds (Mn1–N2 = 2.361 Å and Mn1–N4 = 2.383 Å). The axial Mn–N distances are 0.06 Å longer than those in $[Mn_2(O)_2(TPA)_2]^{2+}$ [41]. This is expected since the quinolyl groups are known to exert steric effects that in turn, prevent the quinolyl nitrogen to approach the manganese centre too closely. Similar structural distinctions have previously been noted in Fe_2O_2 diamond core motifs bearing TPA and 6-Me_3-TPA (6-Me_3-TPA = tris(6-methyl-2-pyridylmethyl)amine) [42].

Addition of manganese(II) acetate to an acetonitrile solution of TQA under N_2 and subsequent addition of sodium perchlorate followed by diethyl ether resulted in a white precipitate. Preliminary characterization allowed us to formulate the complex as $[Mn_2(TQA)_2(\mu\text{-}OAc)_2](ClO_4)_2$ (**2**). The ESI mass spectra for complex **2** in acetonitrile shows a major peak at 553.87 *m/z* which corresponds to the fragment $[Mn_2^{II}(TQA)_2(OAc)_2]^{2+}$ (calculated = 554.1) (Fig. S3). However, ESI-MS analysis in acetonitrile revealed two additional ion peaks at mass to charge (*m/z*) of 511.9 and 589.87 whose mass and isotope distribution patterns correspond to $[Mn_2^{II}(TQA)_2(O)(OH_2)]^{2+}$ (calculated = 512.1) and $[Mn^{II}(TQA)(OAc)(OH_2)_2]^{+}$ (calculated = 590.1), respectively. The results indicate the lability of the bridging acetate anions in **2**. The difference between the asymmetric and symmetric stretching frequencies (88 cm^{-1}, $\Delta\upsilon(\upsilon_{asym} - \upsilon_{sym}, COO^-)$ in the FT-IR spectrum of **2** also indicated the presence of bridging acetate anions (Fig. S4) [43].

The solid state structure of **2** was further established by single crystal X-ray crystallography (Fig. 2). Dissolution of the solid in acetonitrile and vapour diffusion of Et_2O afforded suitable crystals for single crystal X-ray diffraction analysis. As shown in Fig. 2, the asymmetric unit contains a diMn^{II} core bridged by two bidentate acetates. Each of these two Mn(II) centres are further coordinated by the tetradenate N4 ligand (TQA) providing distorted octahedral geometries around the metal ions. Selected bond distances and angles are listed in Table 1.

The mononuclear Mn(II) complex, $[Mn^{II}(TQA)(ClO_4)_2]$. 2MeCN (**3**) was obtained by reacting equimolar amounts of manganese(II) perchlorate and TQA in acetonitrile under nitrogen. Complex **3** crystallizes in the triclinic space group *P*-1. Fig. 3 shows the ORTEP diagram along with the selective atom numbering scheme. Selected bond lengths and

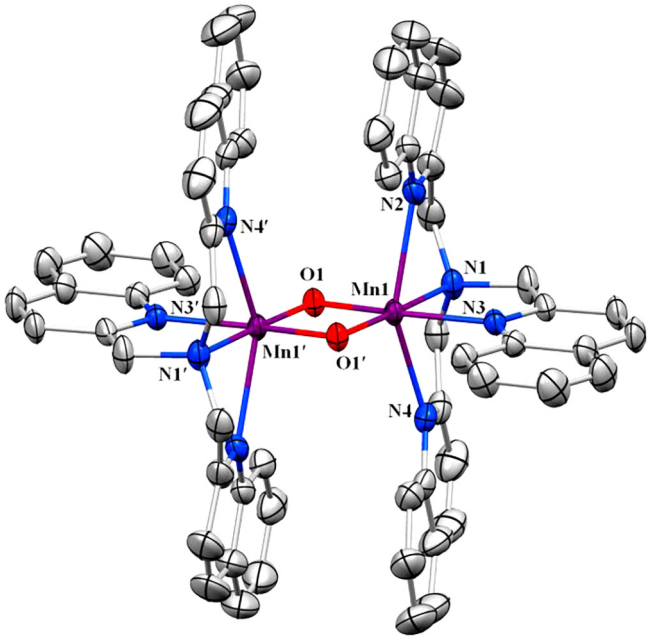

Fig. 1. ORTEP representation of complex **1** (ellipsoids were drawn at 30% probability and the counter cations were omitted for clarity).

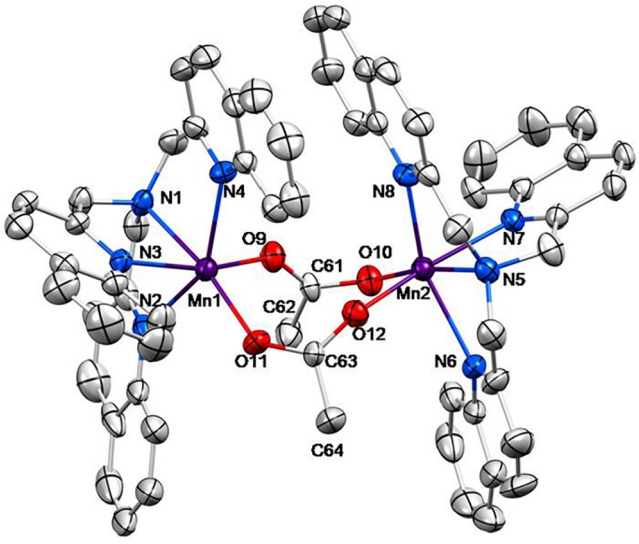

Fig. 2. ORTEP representation of complex **2** (ellipsoids were drawn at 30% probability and the counter cations were omitted for clarity).

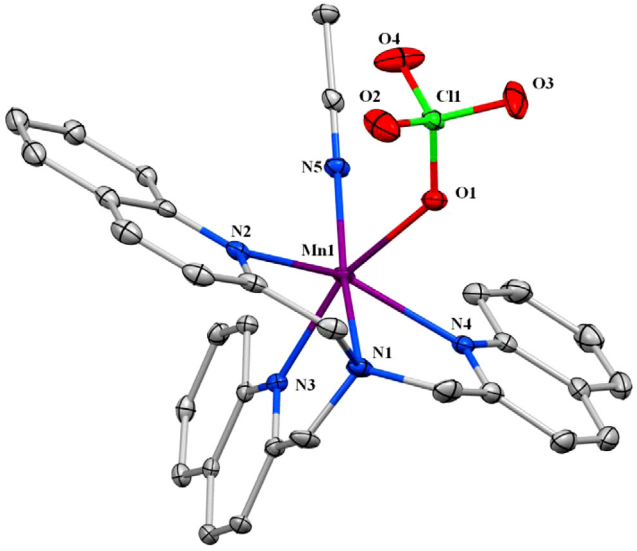

Fig. 3. ORTEP representation of complex **3** (ellipsoids were drawn at 30% probability and the counter cations were omitted for clarity).

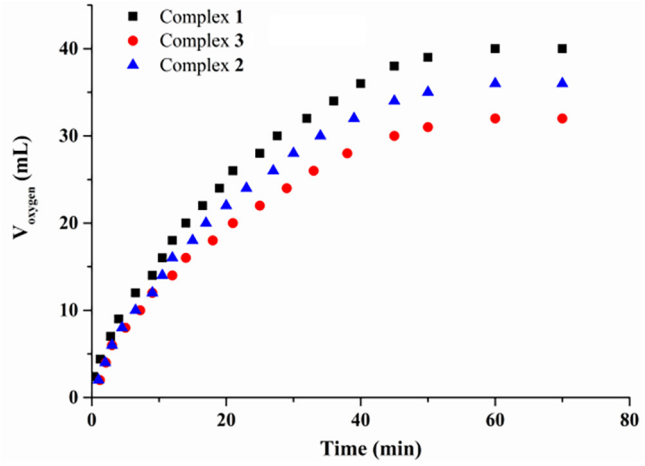

Fig. 4. Volume of oxygen evolved with respect to time upon addition of hydrogen peroxide (1 M) to a solution of complex **1** (black cubes), complex **2** (blue triangles) and complex **3** (red circles) (0.2 mM) in 1:1 methanol:buffer at 20 °C. (For interpretation of the references to colour in this figure legend, the reader is referred to the web version of this article.)

angles have been compiled in Table 1. Complex **3** features a six- coordinated Mn(II) centre with a distorted octahedral coordination sphere enforced by the tetradentate N4 ligand while the axial coordination sites are occupied by a perchlorate and a solvent molecule (acetonitrile). The average Mn–$N_{Quinolyl}$ distance is 2.31 Å while the Mn–N_{amine} distance is 2.23 (Å). These Mn–N distances are typical of high-spin manganese(II) complexes.

3.2. Kinetic studies

As mentioned earlier the oxidized and reduced form manganese catalase contain Mn_2^{III} and Mn_2^{II} core, which is responsible for the catalytic activity. Looking at the similarities between the active sight of the Mn catalase and our synthesized complex we were encouraged to test their abilities to catalytic hydrogen peroxide disproportionation reaction. Upon addition of hydrogen peroxide to solutions of complexes **1** and **2** in 1:1 MeOH/tris-buffer resulted in rapid O_2 evolution indicating that the complexes catalyze H_2O_2 disproportionation. Lack of lag phase indicated that complexes **1** and **2** act as the true catalyst. Evolution of

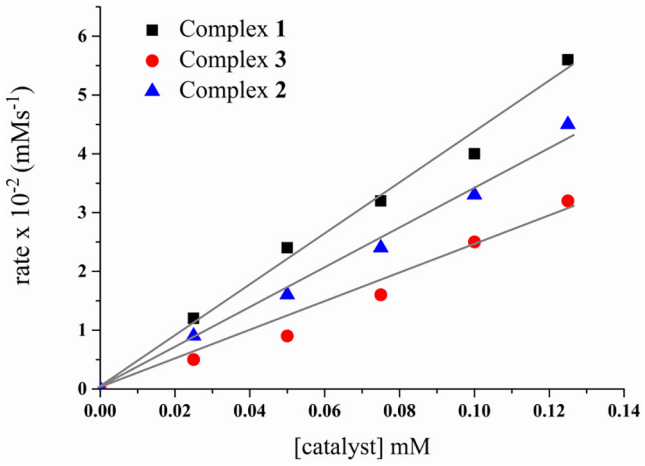

Fig. 5. Initial rate of hydrogen peroxide (100 mM) disproportionation with respect to catalyst concentration. Grey lines indicate linear fitting of data points.

oxygen was measured volummetrically for these complexes and the time profile is given in Fig. 4.

Both complex **1** and complex **2** were able to catalyze hydrogen peroxide giving a turnover number of 810 and 665 mol O_2 per mol of the catalysts, respectively. Reactivity of complex **3** towards catalase activity was also tested and under identical conditions complex **3** was also found to be catalytically active giving a TON of 769. After the first catalytic turnover second batch of H_2O_2 was added to the same catalyst solution of complex **1.** This time the amount of oxygen evolved decreased to half the initial amount indicating degradation of the active catalyst (Fig. S7).

In order to get kinetic parameters 'Initial rate method' was applied by monitoring the amount of oxygen evolved using a Clark type electrode. At constant hydrogen peroxide concentration the initial rate was found to be linearly dependant with the catalyst concentration suggesting a first order dependence with respect to catalyst concentration for all the three complexes (Fig. 5). When concentration of hydrogen peroxide was varied keeping the catalyst concentration fixed a saturation kinetics were observed for all the three catalysts. This implies an equilibrium between the catalyst complex with the substrate. At higher substrate conditions the catalyst-substrate complex remains in large quantity and the rate depends on the decomposition of this complex and free catalyst. This behaviour suggests a Michaelis–Menten type kinetic profile (Fig. 6). Kinetic parameters for the reaction were obtained by fitting the rate vs [H_2O_2] data to the Michaelis–Menten equation.

The values of catalytic turnover number (k_{cat}) and the Michaelis constant (K_M) and catalytic efficiency (k_{cat}/K_M) were determined from the Lineweaver-Burk plot (Fig. 7). The kinetic data are given in Table 3. The value of K_M is a measure of affinity towards the substrate and higher the value lower is the affinity. As evident from the results shown in Table 3, complex **2** has the lowest value of K_M (17 mM) suggesting highest affinity towards the substrate and complex **1** has the lowest affinity having the highest K_M value (90 mM). The *turnover number* k_{cat} is the rate of substrate conversion into the corresponding products and k_{cat}/K_M is the catalytic efficiency. Complex **2** shows the highest catalytic efficiency among these three complexes giving $k_{cat}/K_M = 22\ M^{-1}\ s^{-1}$ which is three times larger than complex **1** ($k_{cat}/K_M = 8.5\ M^{-1}\ s^{-1}$). The activation parameters $\Delta H^{\ddagger} = 35.4\ kJ\ mol^{-1}$ and $\Delta S^{\ddagger} = -86\ J\ K\ mol^{-1}$ for complex **1** was obtained from an Eyring analysis of temperature dependant rate constants (5–25 °C) (Fig. S8).

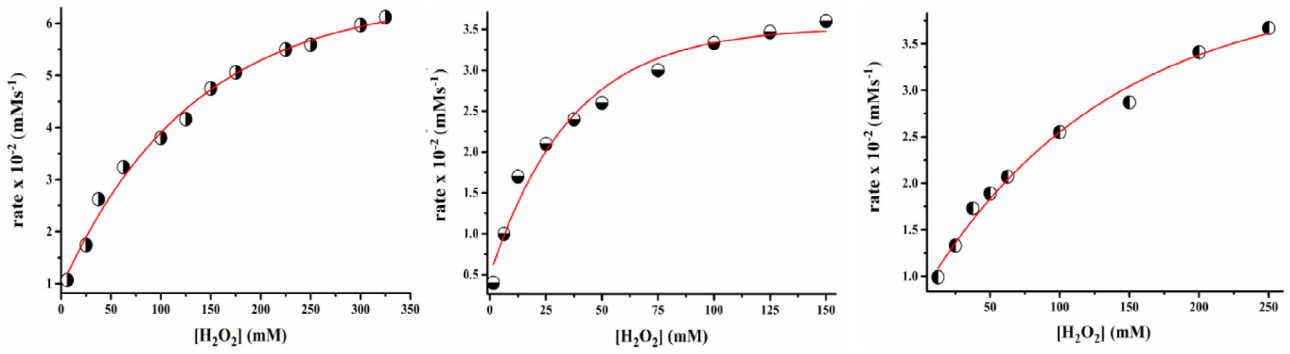

Fig. 6. Plot of initial rate of substrate consumption versus concentration of hydrogen peroxide at fixed catalyst concentration (0.1 mM) at 20 °C. (left for complex **1**, middle for complex **2** and right for complex **3**.)

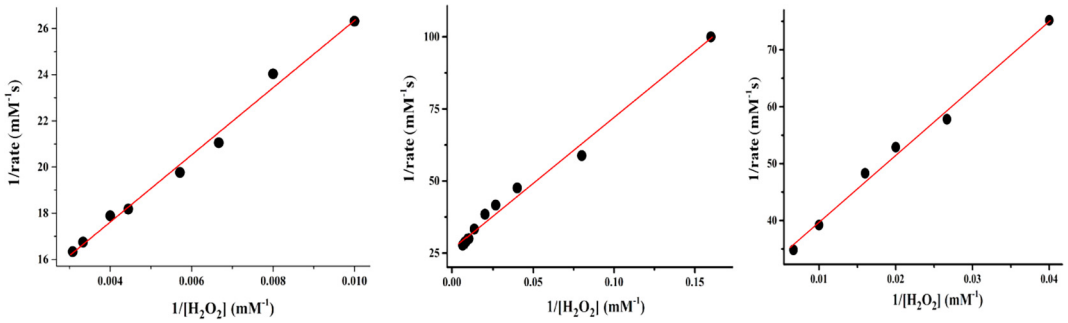

Fig. 7. Lineweaver-Burke plot for complex **1** (left), complex **2** (middle) and complex **3** (right).

Table 3
Comparative table of kinetic data for manganese catalase and different catalase mimics.

Compound	k_{cat}/K_M [$M^{-1}s^{-1}$]	TON	Reaction Condition	Ref.
T. thermophilus catalase	3.1×10^6	n.d.	–	[50]
L. plantarum catalase	0.6×10^6	n.d.	–	[51]
T. album catalase	1.7×10^6	n.d.	PBS (pH 8)	[9]
1	8.5[a]	810[b]	MeOH/tris-buffer	This work
2	22[a]	769[b]	MeOH/tris-buffer	This work
3	7[a]	665[b]	MeOH/tris-buffer	This work
$[Mn_2(bpia)_2(\mu\text{-}OAc)_2](ClO_4)_2$	5.2	n.d.	*N*-Methylformamide	[31]
$[Mn(salpn)O]_2$	1×10^3	n.d.	Acetonitrile	[30]
$[Mn_2(BCPMP)(OAc)_2]$	11.44	7500	Methanol	[49]
$[Mn_2(etsalim)_4(Hetsalim)_2]$ $(ClO_4)_2$	1.6	3150	Methanol (5 equiv NaOH)	[44]
$[Mn_2L_2P_2]^{6+}$	1890	n.d.	BBS (pH 7.8)	[52]
$[Mn_2L_2(Cl)_2]$	2750–7800	n.d	Water	[53]

BBS = Borate Buffer Saline.
[a] Kinetic information was obtained by experiments performed using a Clark type electrode.
[b] TON was determined volumetrically.

3.3. Peroxidase activity

Peroxidase-like activity of the complexes **1–3** was also studied. For these studies oxidation of diammonium salt of ABTS (2,2′-azinobis-(3-ethylbenzothiazoline)-6-sulfonicacid) was followed at pH 6.8 in aqueous solution as it reacts rapidly in presence of a peroxidase catalyst. ABTS is a well known and frequently applied substrate for studying peroxidase like activity. The reduced form of ABTS being colourless and the oxidized form being green makes it very useful in quantifying the peroxide activity [45–47]. The oxidized cation radical of ABTS has very unique spectral feature in the visible region with spectral bands at 415, 650, 735 and 815 nm [45,48]. Addition of H_2O_2 to **1–3** in phosphate buffer (pH 6.8) led to the accumulation of $ABTS^{\cdot +}$ as evident from Fig. 8. The extent of the reaction was measured quantitatively at $\lambda = 650$ nm since $\varepsilon = 12{,}000\ M^{-1}\,cm^{-1}$.

Among these three complex **1** oxidizes only 10% ABTS during the course of the reaction and complex **2** being the least reactive with substrate conversion of 2.5% only. The lower reactivity towards peroxidase probe suggests that these complexes exhibit superior reactivity towards H_2O_2 disproportionation (catalase activity) than oxidation of ABTS (peroxidase activity).

4. Conclusion

In this work we have employed a tripodal quinolyl based ligand TQA (tris(2-quinolylmethyl)amine) to synthesize two novel manganese complexes having structural and functional similarities with the oxidized and reduced form of catalase enzyme. All the complexes were structurally characterized and their reactivity towards H_2O_2 disproportionation reaction were studied. Complex **2**, which is an approximate structural mimic of the reduced form of the Mn-catalases shows the highest catalytic efficiency whereas complex **1** have shown highest turnover number among these three complexes. Further studies to explicitly unravel the reaction mechanism of the diMn catalase

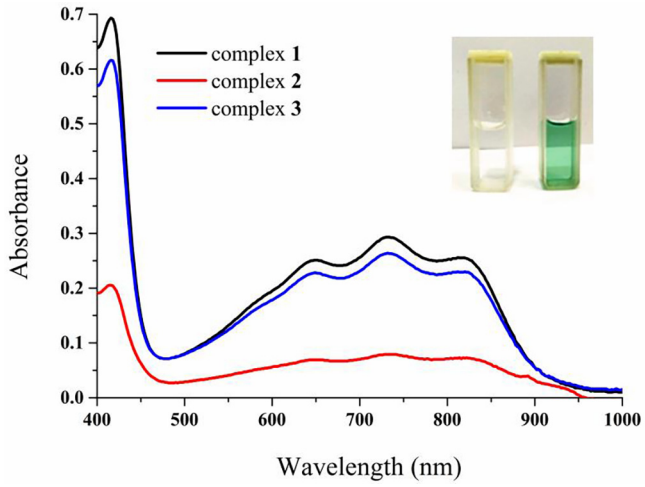

Fig. 8. UV–Vis spectra for the oxidation of ABTS. Inset shows the colour of the solutions before (colourless) and after oxidation of ABTS (green). (For interpretation of the references to colour in this figure legend, the reader is referred to the web version of this article.)

mimics are currently being pursued in the laboratory.

Conflicts of interest

There are no conflicts to declare.

Acknowledgements

This work was supported by grants from the Science and Engineering Research Board (SERB, Project No. YSS/2015/000829 to A.N.B.) & Council of Scientific and Industrial Research (CSIR, Project No. 01(2862)/EMR-II to A.N.B.). A.P. acknowledges research grants from SERB-DST (EEQ/2016/000685) and DST-INSPIRE (DST-INSPIRE/04/2015/002674). S.B. thanks NIT Sikkim for research fellowship.

Appendix A. Supplementary data

Supplementary data to this article can be found online at https://doi.org/10.1016/j.ica.2019.04.015.

References

[1] G.W. Brudvig, Philos. Trans. R. Soc. B: Biol. Sci. 363 (2008) 1211.
[2] J.P. McEvoy, G.W. Brudvig, Chem. Rev. 106 (2006) 4455.
[3] Y. Umena, K. Kawakami, J.-R. Shen, N. Kamiya, Nature 473 (2011) 55.
[4] W.C. Stallings, K.A. Pattridge, R.K. Strong, M.L. Ludwig, J. Biol. Chem. 260 (1985) 16424.
[5] M.W. Parker, C.C. Blake, J. Mol. Biol. 199 (1988) 649.
[6] J.J.P. Perry, D.S. Shin, E.D. Getzoff, J.A. Tainer, Biochim. Biophys. Acta (BBA) – Proteins Proteomics 1804 (2010) 245.
[7] M.W. Vetting, L.P. Wackett, L. Que, J.D. Lipscomb, D.H. Ohlendorf, J. Bacteriol. 2004 (1945) 186.
[8] Y. Kono, I. Fridovich, J. Biol. Chem. 258 (1983) 6015.
[9] G.S. Allgood, J.J. Perry, J. Bacteriol. 168 (1986) 563.
[10] K. Phucharoen, Y. Takenaka, T. Shinozawa, DNA Seq. 12 (2001) 413.
[11] V. Robbe-Saule, C. Coynault, M. Ibanez-Ruiz, D. Hermant, F. Norel, Mol. Microbiol. 39 (2001) 1533.
[12] T. Amo, H. Atomi, T. Imanaka, J. Bacteriol. 184 (2002) 3305.
[13] M. Kolberg, K.R. Strand, P. Graff, K. Kristoffer Andersson, Biochim. Biophys. Acta (BBA) – Proteins Proteomics 1699 (2004) 1.
[14] D.E. Ash, J. Nutr. 134 (2004) 2760S.
[15] J. Bravo, N. Verdaguer, J. Tormo, C. Betzel, J. Switala, P.C. Loewen, I. Fita, Structure 3 (1995) 491.
[16] V.V. Barynin, M.M. Whittaker, S.V. Antonyuk, V.S. Lamzin, P.M. Harrison, P.J. Artymiuk, J.W. Whittaker, Structure 9 (2001) 725.
[17] V.V. Barynin, P.D. Hempstead, A.A. Vagin, S.V. Antonyuk, W.R. Melik- Adamiyan, V.S. Lamzin, P.M. Harrison, P.J. Artymiuk, J. Inorg. Biochem. 67 (1997) 196.
[18] B. Halliwell, J.M.C. Gutteridge, Methods in Enzymology 186 (1990) 1.
[19] B. Halliwell, J.M.C. Gutteridge, Free Radicals in Biology and Medicine, Oxford University Press, 1999.
[20] S.J. Stohs, D. Bagchi, Free Radic. Biol. Med. 18 (1995) 321.
[21] A.J. Wu, J.E. Penner-Hahn, V.L. Pecoraro, Chem. Rev. 104 (2004) 903.
[22] S. Signorellaa, C. Hureau, Coord. Chem. Rev. 256 (2012) 1229.
[23] V. Solís, C. Palopoli, V. Daier, E. Rivière, F. Collin, D.M. Moreno, C. Hureau, S. Signorella, J. Inorg. Biochem. 182 (2018) 29.
[24] M. Kose, P. Goring, P. Lucas, V. Mckee, Inorg. Chim. Acta 435 (2015) 232.
[25] J.-J. Zhang, Q.-H. Luo, C.-Y. Duan, Z.-L. Wang, Y.-H. Mei, J. Inorg. Biochem. 86 (2001) 573.
[26] M. Kose, V. McKee, Polyhedron 75 (2004) 30.
[27] B.-K. Shin, Y. Kim, M. Kim, J. Han, Polyhedron 26 (2007) 4557.
[28] A.E.M. Boelrijk, S.V. Khangulov, G.C. Dismukes, Inorg. Chem. 39 (2000) 3009.
[29] E.J. Larson, V.L. Pecoraro, J. Am. Chem. Soc. 113 (1991) 3810.
[30] E.J. Larson, P.J. Riggs, J.E. Penner-Hahn, V.L. Pecoraro, J. Chem. Soc. Chem. Commun. (1992) 102.
[31] M.U. Triller, W.-Y. Hsieh, V.L. Pecoraro, A. Rompel, B. Krebs, Inorg. Chem. 41 (2002) 5544.
[32] S. Signorella, A. Rompel, K. Bulldt-Karentzopoulos, B. Krebs, V.L. Pecoraro, Jean-Pierre Tuchagues, Inorg. Chem. 46 (2007) 10864.
[33] A.N. Biswas, M. Puri, K.K. Meier, W.N. Oloo, G.T. Rohde, E.L. Bominaar, E. Münck, L. Que, J. Am. Chem. Soc. 137 (2015) 2428.
[34] N. Wei, N.N. Murthy, Q. Chen, J. Zubieta, K.D. Karlin, Inorg. Chem. 1994 (1953) 33.
[35] A. Altomare, G. Cascarano, C. Giacovazzo, A. Guagliardi, J. Appl. Crystallogr. 26 (1993) 343.
[36] G.M. Sheldrick, Acta Crystallogr. Sect. A 64 (2008) 112.
[37] L.J. Farrugia, WinGX Version 1.64, Department of Chemistry, University of Glasgow, 2003.
[38] A. Spek, J. Appl. Crystallogr. 36 (2003) 7.
[39] L. Farrugia, J. Appl. Crystallogr. 30 (1997) 565.
[40] S.R. Cooper, M. Calvin, J. Am. Chem. Soc. 99 (1977) 6623.
[41] L. Dubois, J. Pécaut, M.-F. Charlot, C. Baffert, M.-N. Collomb, A. Deronzier, J.-M. Latour, Chem. Eur. J. 14 (2008) 3013.
[42] E.C. Wilkinson, Y. Dong, Y. Zang, H. Fujii, R. Fraczkiewicz, G. Fraczkiewicz, R.S. Czernuszewicz, L. Que, J. Am. Chem. Soc. 120 (1998) 955.
[43] K. Nakamoto, Infrared and Raman Spectra of Inorganic and Coordination Compounds, fourth ed., Wiley, New York, 1986, p. 231.
[44] M.D. Godbole, M. Kloskowski, R. Hage, A. Rompel, Allison M. Mills, Anthony L. Spek, E. Bouwman, Eur. J. Inorg. Chem. 305 (2005).
[45] E.S. Ryabova, P. Rydberg, M. Kolberg, E. Harbitz, A.-L. Barra, U. Ryde, K.K. Andersson, E. Nordlander, J. Inorg. Biochem. 99 (2005) 852.
[46] B. Eulering, M. Schmidt, U. Pinkernell, U. Karst, B. Krebs, Angew. Chem., Int. Ed. Engl. 1996 (1973) 35.
[47] C.L. Hunter, R. Maurus, M.R. Mauk, H. Lee, E.L. Raven, H. Tong, N. Nguyen, M. Smith, G.D. Brayer, A.G. Mauk, Proc. Natl. Acad. Sci. U.S.A. 100 (2003) 3647.
[48] M.F. Zipplies, W.A. Lee, T.C. Bruice, J. Am. Chem. Soc. 108 (1986) 4433; Q.S. Liu, Trans. Met. Chem. 39 (2014) 917.
[49] R. Singh, M. Haukka, C.J. McKenzie, Ebbe Nordlander, Eur. J. Inorg. Chem. (2015) 3485.
[50] M. Shank, V. Barynin, G.C. Dismukes, Biochemistry 33 (1994) 15433.
[51] J. Penner-Hahn, Manganese Redox Enzymes, VCH Publishers, Inc., New York, 1992, pp. 29–45.
[52] A. Squarcina, A. Sorarù, F. Rigodanza, M. Carraro, G. Brancatelli, T. Carofiglio, S. Geremia, V. Larosa, T. Morosinotto, M. Bonchio, ACS Catal. 2017 (1971) 7.
[53] N. Reddig, D. Pursche, M. Kloskowski, C. Slinn, S.M. Baldeau, A. Rompel, Eur. J. Inorg. Chem. (2004) 879.